Applied Catalysis B: Environmental 92 (2009) 138–153

Contents lists available at ScienceDirect

Applied Catalysis B: Environmental

journal homepage: www.elsevier.com/locate/apcatb

Detailed kinetic modeling of NH_3 SCR over Cu-ZSM-5

Hanna Sjövall [a], Richard J. Blint [b], Louise Olsson [a,*]

[a] Chemical Reaction Engineering and Competence Centre for Catalysis, Chalmers University of Technology, SE-412 96 Göteborg, Sweden
[b] General Motors R&D Center, Chemical and Environmental Sciences Laboratory, 30500 Mound Road, Warren, MI 48090-9055, USA

ARTICLE INFO

Article history:
Received 1 April 2009
Received in revised form 10 July 2009
Accepted 20 July 2009
Available online 28 July 2009

Keywords:
NH_3
Reduction
SCR
Modeling
Zeolite
Cu-ZSM5
NO
Ammonia inhibition

ABSTRACT

A combination of flow reactor experiments and detailed kinetic modeling was used to study the selective catalytic reduction (SCR) of NO_x with NH_3 over Cu-ZSM-5. The model was developed in several steps and the SCR mechanism presented here is based on our earlier work on two subsystems: ammonia storage and ammonia oxidation with and without water, and NO_x adsorption and NO oxidation. In this work, the subsystems were combined with reaction steps for the reduction of nitrogen oxides with ammonia. The SCR mechanism involves a reaction between adsorbed NO_2 and NH_3, formation of HNO_2 and HNO_3 and the final reduction to N_2 or N_2O. Seven experiments that describe the catalytic activity using various feed combinations of NO, NO_2 and NH_3 in both dry and wet feeds were used in the model development. These experiments investigate the SCR of NO over a wide temperature range, the influence of using various NO to NO_2 ratios at 175 °C, the influence of changing NO to NO_2 ratio at 350 °C, the NO oxidation in wet feed, and the ammonia inhibition at low temperature. The model was also validated using six new experiments. The predicted NO_x conversions and formations of N_2O correlated well with the experimental results and show that the detailed kinetic model developed in this study could be used successfully to describe several experimental observations over a wide range of temperatures.

1. Introduction

Emissions from the combustion of fossil fuel contain several pollutants which can be converted over a catalyst to less harmful products. Depending on the conditions during the combustion, various after treatment systems can be used to remove these pollutants. In a lean environment, an efficient way to reduce nitrogen oxides (NO_x), which are one of the major pollutants, is to apply selective catalytic reduction of these oxides with ammonia (NH_3 SCR). The reaction between NH_3 and NO_x occurs continuously on the surface of a catalyst. There are several catalysts investigated for this application. Catalysts composed of vandia supported on titania can be used [1–7], as well as several types of zeolites which are exchanged with metal ions [8–17]. Copper ion-exchanged zeolites have been studied also for other applications, such as the NO decomposition and the selective catalytic reduction of NO_x using hydrocarbons [18–21].

There are several overall reactions that occur over various SCR catalysts during the reduction of NO_x with NH_3. The nitrogen oxides in diesel exhaust are usually composed of a high fraction of NO. Therefore, the main reaction, usually termed the "standard SCR reaction" refers to the one between NO and NH_3 [20,22–27].

$$4NH_3 + 4NO + O_2 \rightarrow 4N_2 + 6H_2O \quad (1)$$

The SCR activity is enhanced as the NO_2 fraction is increased to about equimolar amounts of NO and NO_2. The reduction occurs according to the "fast SCR reaction" [22–24,26].

$$2NH_3 + NO + NO_2 \rightarrow 2N_2 + 3H_2O \quad (2)$$

Both reactions (1) and (2) result in a 1:1 consumption of NO_x and NH_3. The overall reaction with NO_2 is often expressed as a reaction without oxygen [20,23,25].

$$8NH_3 + 6NO_2 \rightarrow 7N_2 + 12H_2O \quad (3)$$

There are several side reactions that compete with the desired reactions. The side reactions can either produce secondary emissions or consume ammonia unproductively. At high temperatures, ammonia may be oxidized to N_2 and possibly even form additional NO_x or N_2O [20]. At temperatures below 200 °C, ammonium nitrate (NH_4NO_3) can be formed, which may subsequently decompose at higher temperatures and possibly contribute to the formation of N_2O [23].

The mechanism that describes the selective catalytic reduction of NO_x with ammonia is not yet fully understood and there are various reaction pathways and reaction intermediates proposed in the literature [8,28–32]. It has been proposed that NO_2 is the reactive species for the SCR of NO_x with NH_3 on zeolite catalysts, and that the oxidation of NO to NO_2 is the rate-limiting step [33]. Stevenson et al. [34] and Wallin et al. [35] suggest that oxidation of NO is the rate determining step in the reduction of NO by NH_3 on H-ZSM-5.

* Corresponding author. Tel.: +46 31 772 4390; fax: +46 31 772 3035.
E-mail address: louise.olsson@chalmers.se (L. Olsson).

0926-3373/$ – see front matter © 2009 Elsevier B.V. All rights reserved.
doi:10.1016/j.apcatb.2009.07.020

Nomenclature list

A_n	monolith wall area in each tank (m^2)
A_j	pre-exponential factor for reaction j (mol/(s $kg_{washcoat}$) or m^3/(s $kg_{washcoat}$))
$c_{g,i,n}$	concentration in the gas phase of component i in tank number n (mol/m^3)
$c_{s,i,n}$	concentration on the surface of the washcoat of component i in tank number n (mol/m^3)
d	channel width (m)
D	diffusion coefficient (m^2/s)
$E_{a,j}$	activation energy for reaction j (J/mol)
$E_{a,j}(0)$	activation energy for reaction j for zero coverage (J/mol)
$F_{i,n}$	molar flow of component i in tank number n (mol/s)
$F_{i,n-1}$	molar flow of component i in tank number $n-1$ (mol/s)
$k_{c,i,n}$	mass transfer coefficient for component i in tank number n (m/s)
k_j	rate constant for reaction j (mol/(s $kg_{washcoat}$) or m^3/(s $kg_{washcoat}$))
$m_{wc,n}$	mass of washcoat in tank n (kg)
N_{cat}	number of active sites per mass washcoat (mol/$kg_{washcoat}$)
R	gas constant (J/(mol K))
Re	Reynolds number
$r_{j,n}$	rate of reaction j in tank n (mol/(s $kg_{washcoat}$))
S1a	Cu-site
S1b	Cu-site
S2	Brönsted acid sites
S3	Weak adsorption sites
Sc	Schmidt number
Sh	Sherwood number
Sh_∞	asymptotic Sherwood number
t	time (s)
T	temperature (K)
z	distance from the entrance of the monolith channel (m)
z_m	dimensionless axial distance for the mass transfer

Greek letters

$\alpha_{i,j}$	coverage dependence for species i in reaction j
θ_i	coverage of specie i
$\nu_{i,j}$	stoichiometric coefficient for component i and reaction j
$\Theta_{i,n}$	coverage of specie i in tank n

Devadas et al. [15] also suggest that zeolite catalysts require NO_2 or the ability to oxidize NO to NO_2 to exhibit SCR activity. For copper ion-exchanged mordenite catalysts, a dual site mechanism which involves a surface reaction between NO and NH_3 adsorbed on two different sites was proposed by Choi et al. [31]. Komatsu et al. [8] present another mechanism which involves the formation of a bridging NO_3 which reacts with NO to form NO_2. The NO_2 then reacts with NH_3 to produce N_2 and H_2O. Eng and Bartholomew [28] propose a mechanism which involves a reaction between NO_2 and a pair of NH_4^+ ions to form an active complex. The active complex then reacts rapidly with NO or NO_2 to form N_2 or N_2O, respectively. They further suggest that the role of copper ions in metal exchanged zeolites is to increase the surface concentration of NO_2. Another proposal is that NO and NO_2 form N_2O_3, which reacts with water to produce HNO_2. The nitrous acid was then believed to be the actual intermediate which reacts with ammonia to form N_2 and H_2O [36]. Yeom et al. [30] proposed a reaction scheme initiated by NO_2 and involving the formation of HNO_2 and HNO_3 over a BaNa-Y catalyst. The reaction between HNO_2 and NH_3 produces N_2 and H_2O via ammonium nitrite, but the reaction between HNO_3 and NH_3 produces NH_4NO_3, which is more stable than NH_4NO_2. They further suggest that NO is able to reduce both HNO_3 and NH_4NO_3 into HNO_2 and NH_4NO_2, respectively, with subsequent formation of N_2 and H_2O. Nova et al. [37] and Ciardelli et al. [6] suggest that similar reactions steps are involved in the selective catalytic reduction of NO and NO_2 with ammonia on vanadia based catalysts. They conclude that ammonium nitrate acts as an intermediate which is accumulated on the catalyst surface at low temperatures, and decomposes to N_2O at higher temperatures if NO is absent. A more detailed reaction mechanism based on the redox properties of vanadium-based catalysts during NH_3 SCR of NO_x has been proposed by Tronconi et al. [7]. Grossale et al. [38] conclude in a recent paper that the oxidation of NO by nitrates is the rate-limiting step in the fast SCR at low temperature. The decomposition of nitrites to nitrogen may then occur via formation of unstable of NH_4NO_2.

There are several global kinetics-based models that describe steady-state conditions during ammonia SCR over various catalyst formations [2,4,34,39–41]. Other models have been developed to account also for transient conditions over vandia based catalysts [42–44], Fe exchanged zeolites [45] and Cu-ZSM-5 [46]. However, there are no detailed kinetic models for NH_3 SCR developed for copper zeolites that account for the storage of ammonia and nitrogen oxide, NO oxidation, the selective catalytic reduction of NO and NO_2 and formation of N_2O, both with and without the presence of water. The objective of this study was to develop a detailed kinetic model for ammonia SCR over Cu-ZSM-5 based on our two earlier studies on the same catalyst that investigates ammonia storage and oxidation [47], and NO adsorption and oxidation [48]. The total mechanism contains a combination of the two subsystems and additional reaction steps for the selective catalytic reduction of nitrogen oxides with ammonia. The aim is to describe not only the ammonia storage, the ammonia and NO oxidation, and the standard SCR activity, but also the effect of various combinations of NO and NO_2 concentrations and the influence of increased ammonia concentrations.

2. Experimental

2.1. Catalyst preparation

The catalysts were prepared using H-ZSM-5 powder with a silica to alumina ratio of 27 obtained from Alsi-Penta. The Cu-ZSM-5 powder was prepared by an ion-exchange method performed in two steps. The H-ZSM-5 powder was ion-exchanged using a $NaNO_3$ solution at ambient temperature, and the ion-exchange to sodium was performed twice. The Na-ZSM-5 obtained was dried in an oven before the copper was introduced at ambient temperature using a $Cu(CH_3COO)_2$ solution. The ion-exchange into copper was performed three times. After the last ion-exchange step, the powder was filtered and washed with distilled water. The Cu-ZSM-5 was then dried in an oven. The aluminum and copper contents were determined by inductively coupled plasma and atomic emission spectrometry (ICP-AES).

The zeolite powder was washcoated on monoliths. The slurry used for the monolith coating was composed of a liquid phase of distilled water and ethanol, and a solid phase containing boehmite and Cu-ZSM-5. A thin layer of alumina was initially washcoated on the catalysts to generate an improved surface for the zeolite

Table 1
Weight and ion-exchange level of the catalyst sample.

Sample	SiO_2/Al_2O_3 ratio	Weight alumina layer (mg)	Weight zeolite washcoat layer (mg)	Cu loading (wt%) [12]	Ion-exchange level (Cu/2 Al) [12]
Cu-ZSM-5-a	27	73	1038	2.03	0.70
Cu-ZSM-5-b	27	78	1010	2.03	0.70

attachment, and the catalysts were calcined before introducing the zeolite layer. The monoliths were coated with the zeolite slurry by immersing the monoliths in the slurry, blowing away the excess slurry, and drying and heating in air. This procedure was repeated several times until the monoliths were coated with the desired amount of washcoat. The catalysts were finally calcined at 550 °C for 3 h. Two Cu-ZSM-5 monoliths were prepared at the same time using the same slurries. They are denoted Cu-ZSM-5-a and Cu-ZSM-5-b. The length and the diameter of the samples were 30 mm and 22 mm, respectively. Details about the ion-exchange and the monolith coating can be found in Ref. [12]. The catalysts weights and the ion-exchange levels are shown in Table 1.

2.2. Flow reactor experiments

Catalyst activities were measured using a flow reactor which consisted of a horizontal quartz tube equipped with a heating coil and insulation. The inner diameter of the tube was 22 mm. A thermocouple was placed in front of the catalyst to control the inlet gas temperature, and a second thermocouple was placed inside the sample to measure the catalyst bed temperature. An Environics 2000 gas mixer was used to control the feed gas composition. The water was added downstream of the mixed gases in an evaporator which was heated to 150 °C. The amount of H_2O added to the feed was controlled by exerting pressure on the container holding the water. A Bio-Rad FTS 3000 Excalibur FTIR spectrometer was used to measure the concentrations of NH_3, NO, NO_2 and N_2O. The nitric oxide concentration was also measured by a chemiluminescence detector (CLD 700) connected to the system. The gas flow and the space velocity were 3500 ml/min and 18,400 h^{-1}, respectively. The catalyst was exposed to 8% O_2 in argon for 20 min at 500 °C and cooled to experimental temperature in Ar prior to each experiment. All experiments were performed at atmospheric pressure and the inert balance was argon. The reactor setup is described in more detail elsewhere [12]. The experiments included in the model development are described below and a summary of the experiments is shown in Table 2.

A variable-temperature experiment was conducted using Cu-ZSM-5-a with 500 ppm NO, 500 ppm NH_3 and 8% O_2 in argon. The catalyst was initially heated to 100 °C and kept at that temperature for 40 min to reach steady-state. The temperature was then increased stepwise up to 500 °C. The catalyst was exposed to the gas mixture at 150 °C and 200 °C for 30 min, and at 250 °C, 300 °C, 350 °C, 400 °C, 450 °C and 500 °C for 20 min at each temperature. A second experiment was carried out over Cu-ZSM-5-a at the same temperatures, but instead using 500 ppm NH_3, 500 ppm NO, 8% O_2 and 5% H_2O.

Experiments using various NO to NO_2 feed concentration ratios were conducted at 175 °C. The feed mixture contained 500 ppm NH_3, 500 ppm total NO_x and 8% O_2. The activity was measured while the catalyst was exposed to a gas mixture with a NO_2 to NO_x fraction equal to zero (i.e., NO only) for 40 min. Then the NO_x reduction activity was measured at NO_2 to NO_x fractions of 20%, 40%, 50% and 60% NO_2 for 20 min at each NO_x fraction. The experiment was carried out both with and without the presence of 5% H_2O and both experiments were conducted over the Cu-ZSM-5-b catalyst. A similar experiment was carried out at 350 °C using Cu-ZSM-5-a and various NO to NO_2 mixtures. The inlet concentration was: 500 ppm NH_3, 500 ppm total NO_x, and 8% O_2. The activity was measured during exposure of the catalyst to the gas mixture at NO_2 to NO_x equal to zero for 30 min. Then the NO_x reduction activity was measured at NO_2 to NO_x fractions consisting of 20%, 40%, 50%, 60%, 80% and 100% NO_2 for 15 min at each NO_2 to NO_x fraction.

Additional experiments were carried out to investigate the effects of the feed concentration of NH_3. Three experiments were carried out at 175 °C and two additional experiments were conducted at 350 °C. In the first experiment the temperature was kept at 175 °C while exposing Cu-ZSM-5-a catalyst to 500 ppm NO, 8% O_2 and 200 ppm NH_3 for 60 min. The concentration of ammonia was then stepwise increased to 300 ppm, 400 ppm, 500 ppm, 600 ppm, 700 ppm and 800 ppm (for 60 min at each ammonia level). The second experiment was performed in a similar way over the same catalyst sample, but in presence of 5% H_2O. The third experiment was conducted over Cu-ZSM-5-b with varying the ammonia concentration accordingly, but the catalyst was exposed to equal amounts of NO and NO_2, thus using 200–800 ppm NH_3, 250 ppm NO, 250 ppm NO_2, 8% O_2 and 5% H_2O. A similar experiment was then carried out at 350 °C using 50–800 ppm NH_3, 500 ppm NO and 8% O_2. The catalyst was initially exposed to a mixture with 50 ppm NH_3 for 30 min and then to 100 ppm, 150 ppm, 200 ppm, 300 ppm, 400 ppm, 500 ppm, 600 ppm, 700 ppm and 800 ppm NH_3 (20 min at each NH_3 level). The same type of experiment was then carried out at 350 °C using equal concentration of NO and NO_2. The feed mixture contained 250 ppm NO, 250 ppm NO_2, 8% O_2 and 50–800 ppm NH_3, and the activity was measured for 20 min at each ammonia concentration. Both experiments at 350 °C were conducted over Cu-ZSM-5-a.

Table 2
Summary of experiments.

Experiment	Composition	Temperature (°C)	Comment
NH_3 SCR of NO	500 ppm NO, 500 ppm NH_3 and 8% O_2	100–500	Used in model development (Fig. 1)
NH_3 SCR of NO	500 ppm NO, 500 ppm NH_3, 8% O_2 and 5% H_2O	100–500	Used in model development (Fig. 2)
NH_3 SCR of NO_x (0–60% NO_2)	500 ppm NO_x, 500 ppm NH_3 and 8% O_2	175	Used in model development (Fig. 3)
NH_3 SCR of NO_x (0–60% NO_2)	500 ppm NO_x, 500 ppm NH_3, 8% O_2 and 5% H_2O	175	Used in model development (Fig. 4)
NH_3 SCR of NO_x (0–100% NO_2)	500 ppm NO_x, 500 ppm NH_3 and 8% O_2	350	Used in model development (Fig. 5)
NH_3 inhibition	200–800 ppm NH_3, 500 ppm NO and 8% O_2	175	Used in model development (Fig. 6)
NO oxidation	500 ppm NO, 8% O_2 and 5% H_2O	100–450	Used in model development (Fig. 7)
NH_3 inhibition	200–800 ppm NH_3, 500 ppm NO, 8% O_2 and 5% H_2O	175	Used in model validation (Fig. 8)
NH_3 SCR of NO (increasing NH_3 concentration)	50–800 ppm NH_3, 500 ppm NO and 8% O_2	350	Used in model validation (Fig. 9)
NH_3 inhibition	200–800 ppm NH_3, 250 ppm NO, 250 ppm NO_2, 8% O_2 and 5% H_2O	175	Used in model validation (Fig. 10)
NH_3 SCR of NO_x (increasing NH_3 concentration)	50–800 ppm NH_3, 250 ppm NO, 250 ppm NO_2 and 8% O_2	350	Used in model validation (Fig. 11)
NH_3 SCR of NO (increasing NO concentration)	500 ppm NH_3, 50–800 ppm NO and 8% O_2	175	Used in model validation (Fig. 12)
NH_3 SCR of NO (increasing NO concentration)	500 ppm NH_3, 50–800 ppm NO and 8% O_2	350	Used in model validation (Fig. 13)

In another set of experiments, the feed concentration of NO was varied, while keeping the concentration of NH_3 constant using the Cu-ZSM-5-a catalyst. The temperature was kept at 175 °C while exposing catalyst to 500 ppm NH_3, 8% O_2 and 50 ppm NO for 30 min. The concentration of NO was then stepwise increased to 100 ppm, 150 ppm, 200 ppm, 300 ppm, 400 ppm, 500 ppm, 600 ppm, 700 ppm and 800 ppm, allowing for 20 min at each NO level. The same experiment was then repeated at 350 °C.

Finally, one NO oxidation experiment was conducted to investigate the influence of water on the NO oxidation activity. The inlet feed was 500 ppm NO, 8% O_2 and 5% H_2O and the temperature was increased stepwise from 100 °C to 450 °C.

3. Catalyst model

3.1. The reactor model

The monolith is described as a series of continuously stirred tank reactors. The theoretical number of elements needed was estimated to about 40 using the dispersion model in combination with the tanks-in-series model [49]. However, using 40 tanks would require very long simulation times and Westerberg et al. [50] used 10 tanks in their HC SCR model, instead of the theoretical number of 40–140. We also chose to use 10 elements in this study. In order to check this assumption a simulation using 12 experiments with 15 elements was conducted. The difference between the errors from the simulation using 10 elements and the errors from the simulation using 15 elements was less than 0.3%. Further, the assumptions made for the reactor model are: (i) no gas phase accumulation, (ii) no diffusion resistance in the washcoat and (iii) no radial concentration gradients. The measured catalyst temperature was used in the simulations and the energy balance was not solved, since the reaction heat associated with NH_3 SCR is very low. Mass-transfer limitation in the washcoat was studied earlier using a similar Cu-ZSM-5 catalyst, and the results indicated that there are no such limitations [46]. The film model was used to describe the external mass transfer from the gas to the surface. The mass transfer coefficient, $k_{c,i,n}$, was calculated using the Sherwood number according to

$$Sh = \frac{k_{c,i,n} d}{D}, \tag{4}$$

where the diffusion coefficient D, is calculated using the Fuller correlation [51]. The following equation was used to estimate the Sherwood number [52]

$$Sh = Sh_\infty + 6.874(1000 z_m)^{-0.488} e^{-57.2 z_m} \tag{5}$$

where Sh_∞ is the asymptotic Sherwood number which was set to 3.0 in this work. The dimensionless axial distance z_m, is given by Eq. (6).

$$z_m = \frac{z}{dReSc} \tag{6}$$

The mass balance for each gas component (i) in each tank (n) is presented by Eq. (7) and the material balances were solved using Matlab.

$$F_{i,n-1} - F_{i,n} - k_{c,i,n} A_n (c_{g,i,n} - c_{s,i,n}) = 0 \tag{7}$$

The surface balances are given by Eqs. (8) and (9).

$$k_{c,i,n} A_n (c_{g,i,n} - c_{s,i,n}) + \sum_j \nu_{i,j} r_{j,n} m_{wc,n} = 0 \tag{8}$$

$$N_{cat} \frac{\partial \Theta_{i,n}}{\partial t} = \sum_j \nu_{i,j} r_{j,n} \tag{9}$$

3.2. The kinetic model

3.2.1. The surface sites

The catalyst surface is thoroughly described in an earlier publication [47]. The amount of copper exchanged into the zeolite was determined using ICP-AES and the result was used to calculate the theoretical number of Cu sites (S1) in the zeolite. The oxidation state of the copper sites likely follows a redox cycle during the selective catalytic reduction of NO_x with NH_3 as proposed by several authors [53–56]. However, the exact nature of the active sites was not studied in this work and a description of the redox properties of the copper sites would require a more thorough investigation. Electron paramagnetic resonance studies (EPR) [57,58] suggest that $[Cu(II)(NH_3)_4]^{2+}$ are formed. This is also supported by DFT calculations conducted by Delabie et al. [59]. We therefore introduced four sites at each copper where ammonia may adsorb. However, NO_2 TPD experiments [48] show that much smaller amounts of NO_2 are adsorbed and a model using one NO_x per copper fits well with the experiments. We therefore chose to introduce one active site per copper, which is denoted S1a, where NO_2, NH_3, O_2 and H_2O can adsorb. In addition, three S1b sites are available on each copper, which results in a total of four NH_3 per copper. According to DFT simulations [59], several water molecules may also bind to each copper. We therefore include both NH_3 and H_2O adsorption on S1b in this model. The catalyst also contains Brönsted acid sites (S2). The number of Brönsted acid (S2) sites was calculated from the known Si/Al ratio and the ion-exchange level (0.70 Si/2 Al). Sites for weakly bound molecules (S3) were also included in the model in order to account for additional weakly bound species (NH_3 and H_2O) on the washcoat. The total number of sites was equal to the amount of ammonia adsorbed at ambient temperature and the number of S1a, S1b, S2 and S3 sites in the catalysts are shown in Table 3. Both Cu-ZSM-5-a and Cu-ZSM-5-b have the same number of sites per washcoat weight, because they are prepared from the same zeolite powder. They were also prepared at the same time with the same slurry and have similar zeolite masses (1038 mg and 1010 mg). Further, the conversion of NO was similar over both catalysts (only about 5 ppm difference) after initial stabilization.

This ammonia SCR model is based on two sub-models developed on the same catalysts. The first sub-model describes ammonia adsorption, desorption and oxidation [47]. The second sub-model accounts for NO_x adsorption and NO oxidation [48]. In this work, additional SCR steps are included in the mechanism to describe the NO_x reduction activity using ammonia as reducing agent.

3.2.2. The kinetic model for NH_3, H_2O and O_2 adsorption and the NH_3 oxidation

The model includes reaction steps for adsorption on and desorption from all sites available. The Cu-ZSM-5 catalysts are modeled using copper sites (S1a and S1b), Brönsted acid sites (S2) and additional sites for weakly bound species (S3) [47]. The model also accounts for reaction steps for adsorption and desorption of oxygen on copper sites (S1a). The oxygen is assumed to adsorb molecularly and then dissociate to oxygen atoms on the surface [48]. The details about ammonia oxidation are not well understood and a single-step reaction between NH_3 adsorbed on the S1b site

Table 3
Number of sites used in the model.

Sample	Cu-sites, S1a ($mol/kg_{washcoat}$)	Cu-sites, S1b ($mol/kg_{washcoat}$)	Brönstedt acid sites, S2 ($mol/kg_{washcoat}$)	Weak adsorption sites, S3 ($mol/kg_{washcoat}$)
Cu-ZSM5-a	0.320	0.959	0.288	1.227
Cu-ZSM5-b	0.320	0.959	0.288	1.227

Table 4
Reaction and rate expressions for NH_3, H_2O and O_2 adsorption and desorption and the NH_3 oxidation.

No	Reaction	Reaction rates
1	$NH_3 + S1a \underset{r_{1,b}}{\overset{r_{1,f}}{\longleftrightarrow}} NH_3 - S1a$	$r_{1,f} = k_{1,f} c_{NH_3} \theta_{S1a-vacant}$ $r_{1,b} = k_{1,b} \theta_{NH_3-S1a}$
2	$NH_3 + S1b \underset{r_{2,}}{\overset{r_{2,f}}{\longleftrightarrow}} NH_3 - S1b$	$r_{2,f} = k_{2,f} c_{NH_3} \theta_{S1b-vacant}$ $r_{2,b} = k_{2,b} \theta_{NH_3-S1b}$
3	$NH_3 + S2 \underset{r_{3,b}}{\overset{r_{3,f}}{\longleftrightarrow}} NH_3 - S2$	$r_{3,f} = k_{3,f} c_{NH_3} \theta_{S2-vacant}$ $r_{3,b} = k_{3,b} \theta_{NH_3-S2}$
4	$NH_3 + S3 \underset{r_{4,b}}{\overset{r_{4,f}}{\longleftrightarrow}} NH_3 - S3$	$r_{4,f} = k_{4,f} c_{NH_3} \theta_{S3-vacant}$ $r_{4,b} = k_{4,b} \theta_{NH_3-S3}$
5	$H_2O + S1a \underset{r_{5,b}}{\overset{r_{5,f}}{\longleftrightarrow}} H_2O - S1a$	$r_{5,f} = k_{5,f} c_{H_2O} \theta_{S1a-vacant}$ $r_{5,b} = k_{5,b} \theta_{H_2O-S1a}$
6	$H_2O + S1b \underset{r_{6,b}}{\overset{r_{6,f}}{\longleftrightarrow}} H_2O - S1b$	$r_{6,f} = k_{6,f} c_{H_2O} \theta_{S1b-vacant}$ $r_{6,b} = k_{6,b} \theta_{H_2O-S1b}$
7	$H_2O + S2 \underset{r_{7,b}}{\overset{r_{7,f}}{\longleftrightarrow}} H_2O - S2$	$r_{7,f} = k_{7,f} c_{H_2O} \theta_{S2-vacant}$ $r_{7,b} = k_{7,b} \theta_{H_2O-S2}$
8	$H_2O + S3 \underset{r_{8,b}}{\overset{r_{8,f}}{\longleftrightarrow}} H_2O - S3$	$r_{8,f} = k_{8,f} c_{H_2O} \theta_{S3-vacant}$ $r_{8,b} = k_{8,b} \theta_{H_2O-S3}$
9	$O_2 + S1a \underset{r_{9,b}}{\overset{r_{9,f}}{\longrightarrow}} O_2 - S1a$	$r_{9,f} = k_{9,f} c_{O_2} \theta_{S1a-vacant}$ $r_{9,b} = k_{9,b} \theta_{O_2-S1a}$
10	$O_2 - S1a + S1a \underset{r_{10,b}}{\overset{r_{10,f}}{\longleftrightarrow}} 2O - S1a$	$r_{10,f} = k_{10,f} \theta_{O_2-S1a} \theta_{S1a-vacant}$ $r_{10,b} = k_{10,b} \theta^2_{O-S1a}$
11	$2NH_3 - S1b + 3O - S1a \xrightarrow{r_{11}} N_2(g) + 2H_2O - S1b + H_2O - S1a + 2S1a$	$r_{11} = k_{11} \theta_{NH_3-S1b} \theta_{O-S1a}$
12	$H_2O - S1a + O - S1a \underset{r_{12,b}}{\overset{r_{12,f}}{\longleftrightarrow}} 2OH - S1a$	$r_{12,f} = k_{12,f} \theta_{O-S1a} \theta_{H_2O-S1a}$ $r_{12,b} = k_{12,b} \theta^2_{OH-S1a}$
13	$2NH_3 - S1b + 2O - S1a + 2OH - S1a \xrightarrow{r_{13}} N_2(g) + 2H_2O - S1b + 2H_2O - S1a + 2S1a$	$r_{13} = k_{13} \theta_{NH_3-S1b} \theta_{O-S1a} \theta_{OH-S1a}$

and oxygen adsorbed on the S1a site was therefore assumed in the model [47]. Experimentally we observed that the NH_3 oxidation is only slightly decreased when adding water [12]. However, the NO oxidation capacity decreases significantly and we propose that the decreased NO oxidation activity is caused by formation of high coverage of OH groups on the surface (see Section 4). These hydroxyls also block the ammonia oxidation in the simulations. However, experimentally, the ammonia oxidation was only affected by water to a small degree, and we therefore introduced one extra reaction step, where ammonia is oxidized by OH and O on the surface [47]. Table 4 shows the mechanism and reaction rates for adsorption and desorption of ammonia, water and oxygen and the two steps for ammonia oxidation.

3.2.3. The kinetic model for NO_x adsorption and NO oxidation

A detailed description of the NO_x mechanism included in this model has been reported by Olsson et al. [48] in earlier work, and the reaction steps are shown in Table 5. Briefly, the model includes steps for adsorption and desorption of NO_2 on both copper sites (S1a) and Brönsted acid sites (S2). Nitric oxide is assumed to oxidize according to an Eley-Rideal type of mechanism involving gas phase NO molecules. In a previous DRIFT study, we observed large formation of nitrites/nitrates on the surface [14]. Further, NO release was observed when exposing the catalyst to NO_2 only, which likely is due to the reaction between two NO_2 to form NO and nitrates. One reversible reaction was therefore added to describe the formation of NO + NO_3 from NO_2. However, experimentally it is observed that the nitrates can decompose without the presence of NO and we therefore introduced one reversible reaction step for the decomposition of nitrates. The summation of the two reaction steps included in the model results in the global step below.

$$3NO_2{-}S1a + O{-}S1a \leftrightarrow 2NO_3{-}S1a + NO(g) + 2S1a$$

Indeed, the stoichiometry of 1 mol NO produced for every 3 mol NO_2 adsorbed correlates well with the experimental observations. This is also in line with the mechanism proposed by Grossale et al. [60] for a Fe zeolite.

$$3NO_2{-}O^{2-} \leftrightarrow 2NO_3{}^{-}{-} + NO$$

The sub-model developed by Olsson et al. [48] includes reactions for low temperature NO oxidation as well, but the low temperature steps were not important in the SCR mechanism since the reduction activity is very low below 150 °C. Thus, in order to keep the model as simple as possible, the steps for low temperature NO oxidation were excluded in our SCR model.

Table 5
Reaction and rate expressions for NO_2 adsorption and desorption, NO_3 formation and the NO oxidation.

No	Reaction	Reaction rates
14	$NO_2 + S1a \underset{r_{14,b}}{\overset{r_{14,f}}{\longleftrightarrow}} NO_2 - S1a$	$r_{14,f} = k_{14,f} c_{NO_2} \theta_{S1a-vacant}$ $r_{14,b} = k_{14,b} \theta_{NO_2-S1a}$
15	$NO_2 + S2 \underset{r_{15,b}}{\overset{r_{15,f}}{\longleftrightarrow}} NO_2 - S2$	$r_{15,f} = k_{15,f} c_{NO_2} \theta_{S2-vacant}$ $r_{15,b} = k_{15,b} \theta_{NO_2-S2}$
16	$NO + O - S1a \underset{r_{16,b}}{\overset{r_{16,f}}{\longleftrightarrow}} NO_2 - S1a$	$r_{16,f} = k_{16,f} c_{NO} \theta_{O-S1a}$ $r_{16,b} = k_{16,b} \theta_{NO_2-S1a}$
17	$2NO_2 - S1a \underset{r_{17,b}}{\overset{r_{17,f}}{\longleftrightarrow}} NO_3 - S1a + NO + S1a$	$r_{17,f} = k_{17,f} \theta^2_{NO_2-S1a}$ $r_{17,b} = k_{17,b} \theta_{NO_3-S1a} c_{NO} \theta_{S1a-vacant}$
18	$NO_2 - S1a + O - S1a \underset{r_{18,b}}{\overset{r_{18,f}}{\longleftrightarrow}} NO_3 - S1a + S1a$	$r_{18,f} = k_{18,f} \theta_{NO_2-S1a} \theta_{O-S1a}$ $r_{18,b} = k_{18,b} \theta_{NO_3-S1a} \theta_{S1a-vacant}$

3.2.4. The kinetic model for NH_3 SCR

The two sub-models above are used in combination with four reaction rates for the reduction of NO_x with NH_3. A summary of the SCR reactions is shown in Table 6. The role of NO and NO_2 has been a subject to many studies concerning the selective catalytic reduction with ammonia. The formation of NO_2 was suggested to be the rate-determining step in the reduction of NO by ammonia over H-ZSM-5 [34,35]. Komatsu et al. [8] suggest a mechanism for the SCR with NH_3 over copper ion-exchanged zeolites, which is initiated by a reaction between NO_2 and NH_3 adsorbed at the same copper site. In our mechanism, such a reaction is modeled by a reaction between NO_2 on S1a and NH_3 on S1b, since S1a and S1b represents sites on the same copper. It is also possible that NO_2 may react with ammonia adsorbed on other nearby positions (S2), but in order to keep the model as simple as possible, the model includes a reaction with ammonia on S1b only.

$$NO_2 - S1a + NH_3 - S1b \xrightarrow{r_{19}} H_2O - S1b + OH - S1a + N_2$$

Komatsu et al. [8] proposed a step for dehydration of two OH groups in their mechanism for the SCR of NO on copper sites. Such a step was introduced as a reversible reaction in our NH_3 oxidation study [47] and is shown in Table 4 (reaction (12)). Two alternative reactions with the hydroxyl groups are also included in this model. It was observed in our previous study that the adsorption of NO was very low and we assumed that NO is oxidized via an Eley-Rideal reaction [48]. We suggest that the reaction between NO and OH occur accordingly and generates HNO_2 which reacts further with NH_3 to form NH_4NO_2. Moreover, the ammonium nitrite is unstable and decomposes into nitrogen and water. Similar reaction sequences have been described by many authors in earlier work on ammonia SCR. Koebel et al. [26] introduced formation of unstable

Table 6
Summary of reactions and rate expressions for NH_3 SCR.

No	Reaction	Reaction rates
19	$NO_2 - S1a + NH_3 - S1b \xrightarrow{r_{19}} H_2O - S1b + OH - S1a + N_2$	$r_{19} = k_{19} \theta_{NO_2-S1a} \theta_{NH_3-S1b}$
20	$NO + OH - S1a + NH_3 - S1b \xrightarrow{r_{20}} H_2O - S1b + H_2O - S1a + N_2$	$r_{20} = k_{20} c_{NO} \theta_{OH-S1a} \theta_{NH_3-S1b}$
21	$NO_2 - S1a + OH - S1a \underset{r_{21,b}}{\overset{r_{21,f}}{\longleftrightarrow}} HNO_3 - S1a + S1a$	$r_{21,f} = k_{21,f} \theta_{NO_2-S1a} \theta_{OH-S1a}$ $r_{21,b} = k_{21,b} \theta_{HNO_3-S1a} \theta_{S1a-vacant}$
22	$HNO_3 - S1a + NH_3 - S1b \xrightarrow{r_{22}} H_2O - S1a + H_2O - S1b + N_2O$	$r_{22} = k_{22} \theta_{HNO_3-S1a} \theta_{NH_3-S1b}$

NH_4NO_2 from a reaction between HNO_2 and NH_3 as a reaction step in the reduction of NO_2 with ammonia. Yeom et al. [30] also included these reactions in their mechanism developed for a BaNa-Y catalyst and Nova et al. [37,61] suggested a mechanism for the fast SCR over vanadia based catalysts, which involves formation of NH_4NO_2 from the reaction between HNO_2 and NH_3. In our model, the above reactions are included as a summary reaction in order to keep the model as simple as possible (r_{20}).

$$NO + OH - S1a \leftrightarrow HNO_2 - S1a$$
$$HNO_2 - S1a + NH_3 - S1b \leftrightarrow NH_4NO_2 - S1a + S1b$$
$$NH_4NO_2 - S1a + S1b \rightarrow N_2 + H_2O - S1a + H_2O - S1b$$
$$NO + OH - S1a + NH_3 - S1b \xrightarrow{r_{20}} N_2 + H_2O - S1a + H_2O - S1b$$

The second alternative reaction is the reaction between adsorbed NO_2 and the hydroxyls, which produces HNO_3 (r_{21}).

$$NO_2 - S1a + OH - S1a \underset{r_{21,b}}{\overset{r_{21,f}}{\leftrightarrow}} HNO_3 - S1a + S1a$$

Nitric acid may then react with NH_3 to form NH_4NO_3 at temperatures below 200 °C [26]. The formation and decomposition of NH_4NO_3 have been studied thoroughly in the literature [23,26,30,37,61,62]. Ammonium nitrate may dissociate into HNO_3 and NH_3, decompose into N_2O and H_2O, decompose into nitrogen, water and oxygen, or, if NO is present, react with NO to form NO_2 [23]. The contribution from each of the decomposition reactions depends on the conditions such as temperature and heating rate. Ciardelli et al. [62] included in their model for a V-based catalyst a reversible reaction for the formation of NH_4NO_3 from $HNO_3 + NH_3$ and described the formation of N_2O from the reaction between HNO_3 and NH_3. The model presented in this work includes a similar reaction for the formation of N_2O, which is described as a reaction between adsorbed HNO_3 and NH_3 (r_{22}). Formation and storage of ammonium nitrate is also likely to occur at temperatures below 200 °C, but the model does not include a step for the ammonium nitrate formation and is therefore not able to distinguish between $HNO_3 + NH_3$ and NH_4NO_3. The sum of selected reactions in the complete mechanism results in expressions for other possible ammonium nitrate decomposition reactions.

$$HNO_3 - S1a + NH_3 - S1b \xrightarrow{r_{22}} H_2O - S1a + H_2O - S1b + N_2O$$

A summary of all SCR reactions is shown in Table 6. The sum of r_{19} and r_{20} will form the "fast" SCR reaction, $2NH_3 + NO + NO_2 \rightarrow 2N_2 + 3H_2O$. Other pathways, or additional steps such as the NO oxidation, will instead add up to the "standard" SCR reaction.

3.3. The rate parameters

The rate constants are described by the Arrhenius expression.

$$k_j = A_j e^{-E_{a,j}/RT} \quad (10)$$

The parameters for the reactions in the sub-models were presented in our previous work [47,48]. Topsoe et al. [63] and Hunger and Hoffmann [64] states that there are three desorption states for ammonia in H-ZSM-5 with different activation barriers denoted α, β and γ. Further, according to calorimetry the heat of adsorption of ammonia varies between about 70–150 kJ/mol on H-ZSM-5 [65]. In order to simplify the model we use only one site, S2, to represent the Brönsted acid sites, and instead introduced coverage dependent activation energy according to expression (11). Such a surface coverage dependent activation energy was also included in most desorption steps in the sub-models, since the temperature desorption (TPD) experiments resulted in broad desorption peaks which sometimes also contained multiple peaks.

$$E_{a,j} = E_{a,j}(0)(1 - \alpha_{i,j}\theta_i) \quad (11)$$

The parameters not fixed were fitted to the experimental data using the least square method. For reactions were both the pre-exponential factor and the activation energy were fitted, a centered expression was used to describe the rate constant in order to reduce the correlation between the parameters, see Eq. (12). The reference temperature, T_{ref} was set to 600 K.

$$k_j = A_j e^{-(E_{a,j}/R)(1/T - 1/T_{ref})} \quad (12)$$

We observed a large correlation between the parameters for the NH_3 adsorption and oxidation and the SCR reactions. It was therefore important to fit these parameters simultaneously, which was carried out using 13 experiments (NH_3 TPD at 150 °C on HZSM-5, NH_3 TPD at 30 °C and 150 °C on Cu-ZSM-5, H_2O TPD at 150 °C on CuZSM-5, NH_3 oxidation with and without water, NO oxidation with water and six SCR experiments). Seven parameters for the SCR reactions (r_{19}–r_{22}) were fitted and the parameters for the NH_3 storage, H_2O adsorption, and the NH_3 oxidation are reported in our earlier work [47]. The parameters for the reactions included in the NO oxidation study (r_9, r_{10}, and r_{14}–r_{18}) were kept as determined in our earlier work [48]. Regression analysis was performed and the 95% linearized confidence intervals were small compared to the magnitude of the parameter values, indicating that the parameters are well defined. The parameters and the corresponding confidence intervals for all reactions except the seven parameters for the SCR reactions (r_{19}–r_{22}) can be found in our earlier work on ammonia storage and NO oxidation [47,48].

4. Results and discussion

4.1. Ammonia SCR

The ammonia SCR activity was modeled in both dry and humid feed at temperatures from 100 °C to 500 °C. The catalyst (Cu-ZSM-5-a) was exposed to 500 ppm NO, 500 ppm NH_3, 8% O_2, with or without 5% water. The result from the experiment made in dry conditions is shown in the upper panel in Fig. 1. Ammonia is totally stored during the first 20 min, but the storage of NO only occurs for a few minutes. The coverage of NO_2 which is formed from the reaction between NO and O, and the coverage of ammonia increases during the first 20 min since the SCR activity is very low at this temperature, see Fig. 1, lower panel. As the temperature is increased from 100 °C to 150 °C, large amounts of ammonia desorbs from the catalyst surface. Complete conversion of both NO and NH_3 is reached at 200 °C. At this temperature, the coverage of NO_2 is very low since the reaction between NO_2 and NH_3 (r_{19}) is rapid. The reduction of NO declines from 300 °C, but complete conversion of ammonia is retained throughout the experiment since ammonia oxidation is active in the high temperature region. The oxidation of ammonia in combination with low storage capacity results in low coverage of ammonia at 350 °C and above. The complete adsorption of ammonia during the first 20 min is captured by the model, and the model also describes the ammonia desorption adequately. In addition, the calculated steady-state conversion of NO and NH_3 correlates well with the measured concentration. One additional experiment was carried out with Cu-ZSM-5-a using wet feed (5% H_2O) and the result is shown in Fig. 2. Less ammonia is stored in presence of water than in dry feed, which was also observed in earlier NH_3 TPD experiments [47]. The catalytic activity is enhanced by the presence of water at both high and low temperatures and the predicted coverage of OH species on copper is increased. The enhanced activity is described in the model by the reduction of NO via formation of HNO_2 (r_{20}) which becomes more important as the coverage of OH species increases. The model captures the

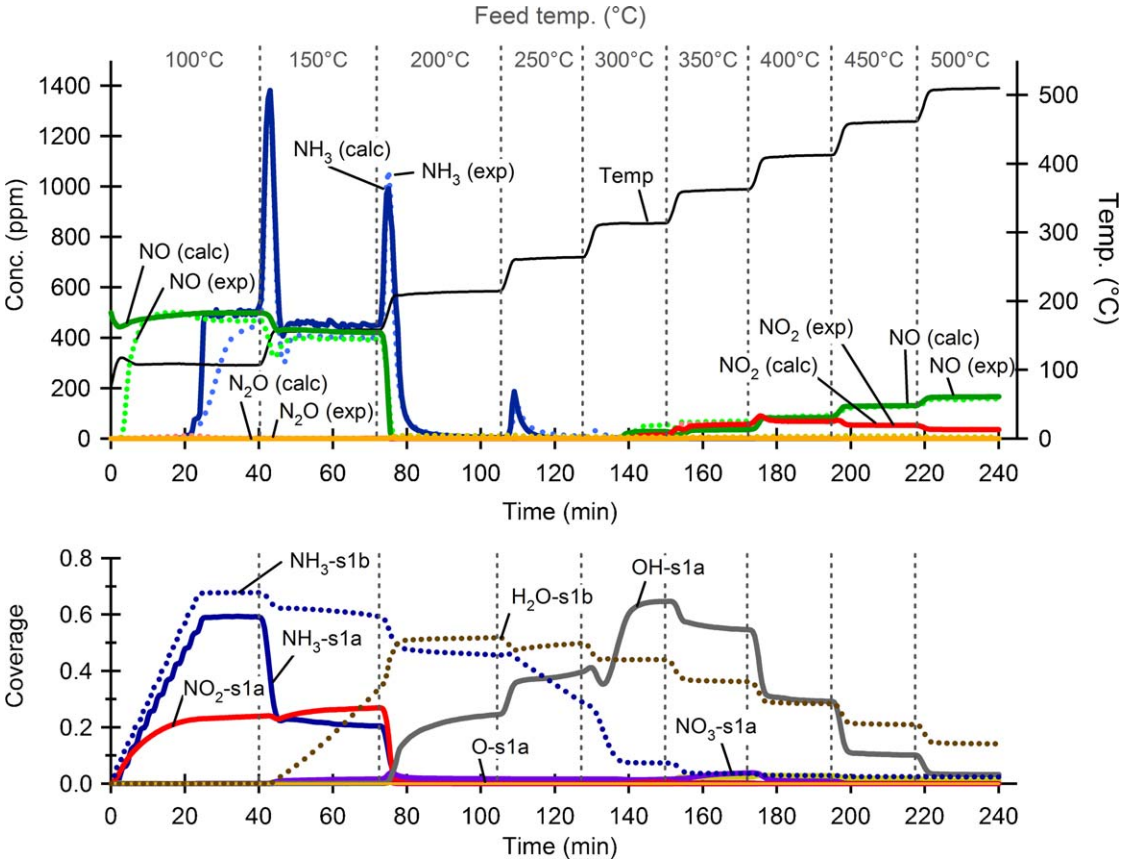

Fig. 1. Upper panel: Measured and calculated concentrations during NH_3 SCR experiment in dry feed using Cu-ZSM-5-a. Feed condition: 500 ppm NH_3, 500 ppm NO and 8 % O_2. The temperature was raised in steps from 100 °C to 500 °C. Dotted lines show the measured concentration and solid lines show the calculated concentration. Lower panel: Calculated mean coverage on S1a and S1b.

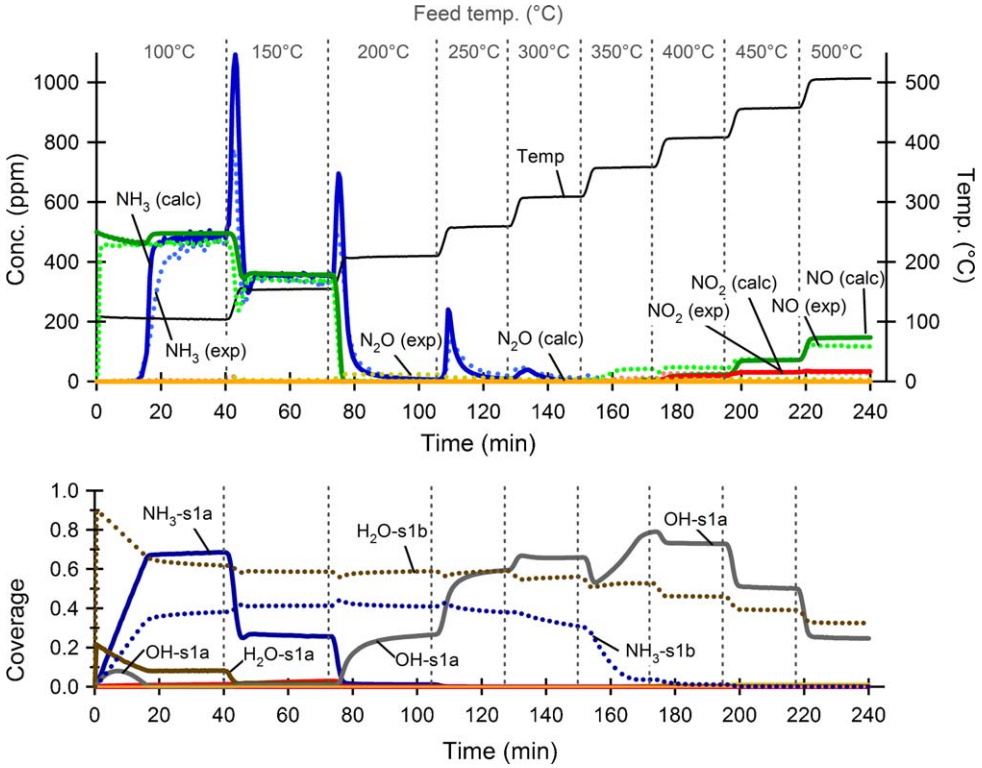

Fig. 2. Upper panel: Measured and calculated concentrations during NH_3 SCR experiment in humid feed using Cu-ZSM-5-a. Feed condition: 500 ppm NH_3, 500 ppm NO, 8% O_2 and 5% H_2O. The temperature was raised in steps from 100 °C to 500 °C. Dotted lines show the measured concentration and solid lines show the calculated concentration. Lower panel: Calculated mean coverage on S1a and S1b.

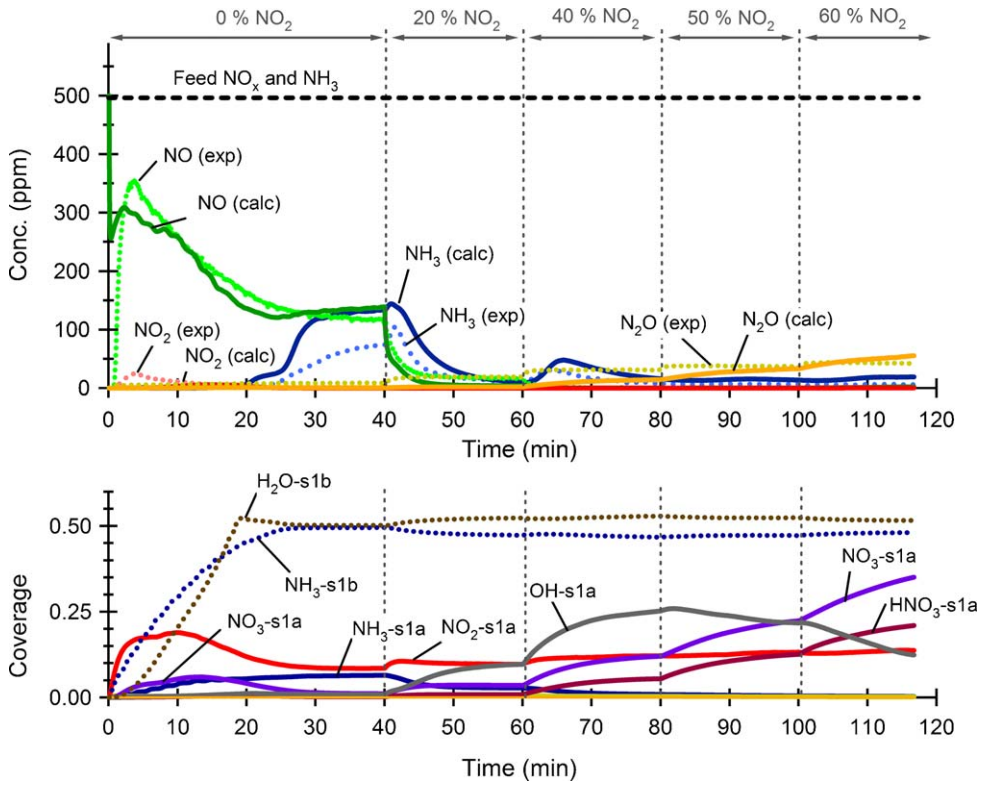

Fig. 3. Upper panel: Measured and calculated concentrations during NH_3 SCR experiment varying the NO to NO_2 ratio in dry feed at 175 °C using Cu-ZSM-5-b. Feed condition: 500 ppm NH_3, 500 ppm NO_x and 8% O_2. Dotted lines show the measured concentration and solid lines show the calculated concentration. Lower panel: Calculated mean coverage on S1a and S1b.

reduced storage of ammonia as well as the enhanced NO_x conversion.

Two temperatures were chosen for further studies: a low temperature (175 °C) where the conversion of NO_x is influenced by a high coverage of ammonia, and a high temperature where the ammonia oxidation is rapid (350 °C). An experiment varying the NO to NO_2 ratio was used in the parameter estimation. The Cu-ZSM-5-b catalyst was exposed to 500 ppm NO, 500 ppm NH_3 and 8% O_2 at 175 °C for 40 min. The NO_x mixture was then changed in steps to include 20%, 40%, 50% and 60% NO_2 for 20 min at each NO to NO_2 ratio. Higher fractions of NO_2 were not used in the simulations due to the possibility of ammonium nitrate formation in the tubing at this low temperature, which makes the experimental results uncertain. This was observed by Ciardelli et al. [6], who found that ammonium nitrate deposits in cold parts of the experimental setup if high fractions of NO_2 are used. The experimental and calculated NH_3, NO, NO_2 and N_2O concentrations are shown in Fig. 3. During the first 40 min NO is used as a NO_x source, and the conversion of NO_x increases gradually during this time. Ammonia adsorbs on the surface and the increased NO conversion follows the change in surface coverage of ammonia since an increased coverage on S1b is beneficial for the reduction of NO_x by NH_3 at this low coverage (r_{19} and r_{20}). The number of OH species are also reduced since r_{20} becomes more rapid. The conversion of NO_x increases as more NO_2 is introduced to the feed. This is due to the rapid SCR, which in our detailed model is described by the combination of r_{19} and r_{20}. The formation of N_2O is also enhanced due to the increased coverage of HNO_3 on the surface. The model can describe all experimental observations well.

The experiment using various NO to NO_2 ratios at 175 °C was also carried out in presence of H_2O and used in the model development. The Cu-ZSM-5-b catalyst was exposed to the same feed mixture as in Fig. 3, except for the addition of 5% H_2O. Fig. 4 shows that the SCR activity is enhanced by the presence of water during the first 40 min, and the NO_x conversion increases as NO_2 is introduced and reaches 100% at equal amounts of NO and NO_2. The formation of N_2O increases with higher fractions of NO_2. The model describes a low, but increasing N_2O formation, as well as the enhanced NO_x conversion activity with higher NO_2 fractions.

The NO to NO_2 ratio was varied also at 350 °C. The catalyst (Cu-ZSM-5-a) was initially exposed to 500 ppm NO, 500 ppm NH_3 and 8% O_2 for 30 min, and then the NO_x composition was changed in steps from 0% to 100% NO_2 (15 min at each composition). Fig. 5 shows a high NO_x conversion at all ratios investigated, and only a small change in activity was observed as the ratio was varied. The highest conversion was achieved close to stoichiometric amounts of NO and NO_2. The model predicts the small change in conversion of both NO_x and NH_3 well at each NO to NO_2 ratio. The formation of N_2O increases with higher NO_2 feed concentration which is captured by the model. A similar experiment was conducted in our earlier work using DRIFT spectroscopy [14]. Based on the FTIR results, we suggested that NO is involved in the SCR, possibly as a gas phase species. Nitric oxide was therefore included as a gas phase species (r_{20}) in the model. The DRIFT spectroscopy result also indicated that high NO_2 to NO fractions leads to increased coverage of nitrites or nitrates on the surface. The surface coverage predicted by our model shows an enhanced NO_3 formation as the feed NO_2 fraction increases. Nitric oxide is involved in several reactions in this mechanism. It is involved in the formation of NO_2 on the surface (r_{16}), and in the reaction with NH_3 via formation of HNO_2 (r_{20}), but also in the reduction of NO_3 (r_{17}). The lower panel in Fig. 5 shows an increased coverage of NO_3 with higher fractions of NO_2 in the feed. A high fraction of NO_2 facilitates formation of NO_3 and if little or no NO is available, reduction of NO_3 becomes slow. This was also observed by Grossale et al. [38], who concluded that the

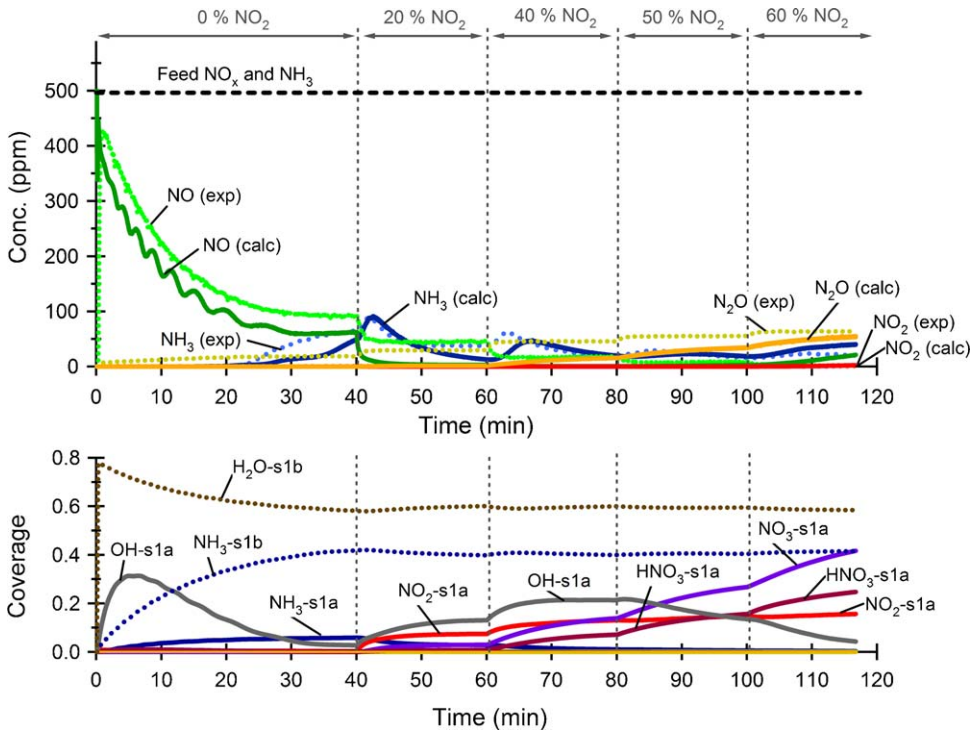

Fig. 4. Upper panel: Measured and calculated concentrations during NH_3 SCR experiment varying the NO to NO_2 ratio in wet feed at 175 °C, using Cu-ZSM-5-b. Feed condition: 500 ppm NH_3, 500 ppm NO_x, 8% O_2 and 5% H_2O. Dotted lines show the measured concentration and solid lines show the calculated concentration. Lower panel: Calculated mean coverage on S1a and S1b.

reduction of nitrates by NO is the rate-limiting step in the fast SCR at low temperatures.

The ammonia inhibition was investigated in dry feed using 500 ppm NO, 8% O_2 and 200–800 ppm NH_3 at 175 °C over Cu-ZSM-5-a. The concentration of ammonia was increased in steps, with 60 min allowed at each level. The conversion of NO increases initially as NH_3 is added to the inlet feed, but at NH_3 concentrations higher than 400 ppm NH_3, the NO_x reduction activity decreases (Fig. 6). The NH_3 is strongly adsorbed on the surface, and high ammonia coverage may cause the decrease in NO conversion, since

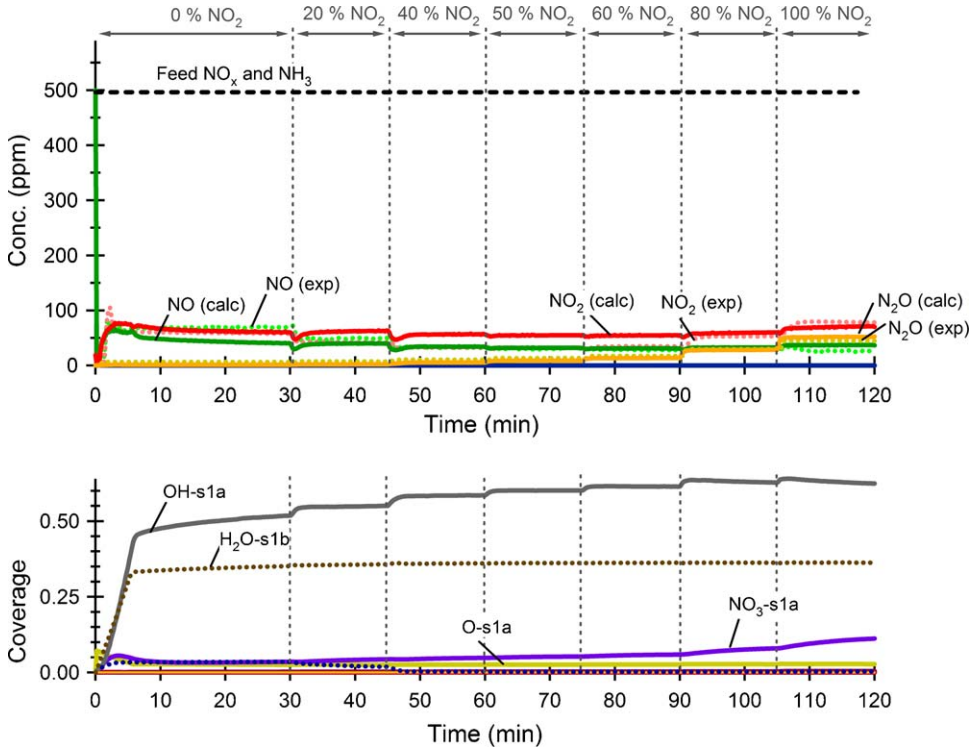

Fig. 5. Upper panel: Measured and calculated concentrations during NH_3 SCR experiment varying the NO to NO_2 ratio in dry feed at 350 °C, using Cu-ZSM-5-a. Feed condition: 500 ppm NH_3, 500 ppm NO_x and 8% O_2. Dotted lines show the measured concentration and solid lines show the calculated concentration. Lower panel: Calculated mean coverage on S1a and S1b.

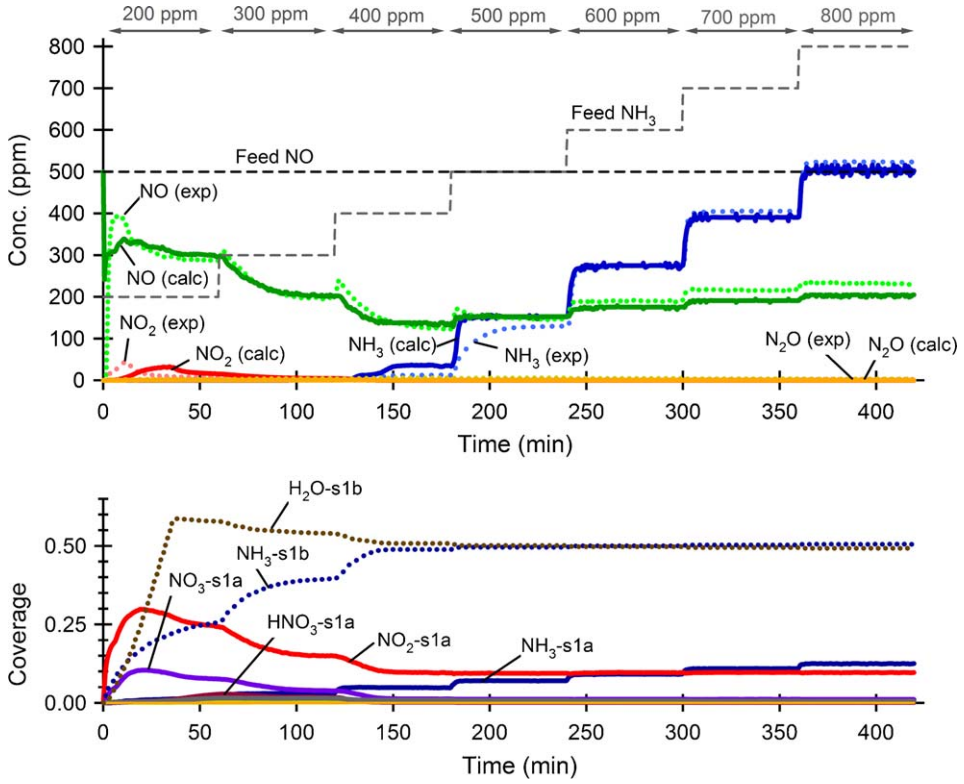

Fig. 6. Upper panel: Measured and calculated concentrations during NH_3 SCR experiment increasing the inlet NH_3 concentration in steps in dry feed at 175 °C using Cu-ZSM-5-a. Feed condition: 200–800 ppm NH_3, 500 ppm NO and 8% O_2. Dotted lines show the measured concentration and solid lines show the calculated concentration. Lower panel: Calculated mean coverage on S1a and S1b.

fewer active sites become available for other reactions which are important for the reduction of NO. This is shown in the lower panel in Fig. 6 where the coverage of NH_3 increases as more ammonia is fed to the reactor. The reduced activity at high NH_3 to NO ratios also results in a slightly decreased coverage of water since less of it is formed as the reduction activity decreases. We observed the same effect in our earlier study using DRIFT spectroscopy [14], where the coverage of water and nitrite or nitrate species decreased while the coverage of ammonia increased as the feed concentration of NH_3 exceeded the inlet concentration of NO. The model captures the inhibition at 500 ppm NH_3 well, and also predicts further blocking effects at higher ammonia fractions.

Finally, one experiment was used to investigate the NO oxidation in presence of water. We have earlier observed a significant decreased NO oxidation when adding water [12]. This decreased NO oxidation is important to capture in order to get a complete SCR model, since the SCR activity is affected by the NO to NO_2 ratio. The catalyst was exposed to 500 ppm NO, 8% O_2 and 5% H_2O and the temperature was increased in steps. The result is shown in Fig. 7. The NO oxidation is very low at temperatures up to 300 °C, but at 350 °C more NO_2 is formed and the oxidation of NO continues to increase at each additional level. There are two possible explanations for the decreased oxidation in presence of water. It is either due to large formation of HNO_3, or formation of OH on the copper sites. However, when increasing the temperature, only small desorption peaks are observed. If large quantities of HNO_3 was stored on the surface, desorption peaks would be visible at each temperature increase, either as HNO_3 or NO_x, as was observed during the dry experiment [48]. Thus, we propose that the decreased NO oxidation activity when adding water is due to formation of OH groups on the surface. The model can describe the reduced NO oxidation in presence of water, which is caused by a large coverage of OH-groups on the surface sites.

4.2. Validation

The model was validated using six additional experiments not included in the model development. The validation experiments were carried out at either 175 °C or 350 °C, varying the concentration of feed NO, NO_2 or NH_3, with or without the presence of water.

The ammonia inhibition was investigated experimentally in wet feed as well as in dry feed in our earlier experimental study on Cu-ZSM-5 [12]. It was observed that water suppresses the ammonia inhibition effect. The decreased ammonia inhibition effect results in enhanced NO reduction activity if equal or higher amounts of ammonia are used in presence of water. Fig. 6 shows the ammonia inhibition in dry feed and Fig. 8 presents the validation experiment in presence of 5% H_2O. The reduced inhibition in wet feed is well described by the model and results in an enhanced NO conversion compared to the conversion in dry feed at inlet concentrations at and above 500 ppm NH_3. The presence of water facilitates formation of OH species and therefore also the reduction of NO via formation of HNO_2 and NH_4NO_2 (r_{20}). The competition for active sites where NO_2 can be formed is thus less important if water is present in the feed.

A similar experiment was carried out at 350 °C where the ammonia oxidation is rapid and the coverage of ammonia is low. An increased feed concentration of ammonia is thus expected to result in enhanced NO reduction at this high temperature. The catalyst (Cu-ZSM-5-a) was exposed to 500 ppm NO, 8% O_2, and a stepwise increased concentration of NH_3 from 50 ppm to 800 ppm. The result is shown in Fig. 9. The conversion of NO_x increases as more ammonia is added to the feed and at 800 ppm NH_3 almost all NO_x is consumed and no ammonia is observed at the reactor outlet. The coverage of ammonia is low and the reduction of NO_x is limited by the amount of ammonia available. At the highest NH_3 fractions,

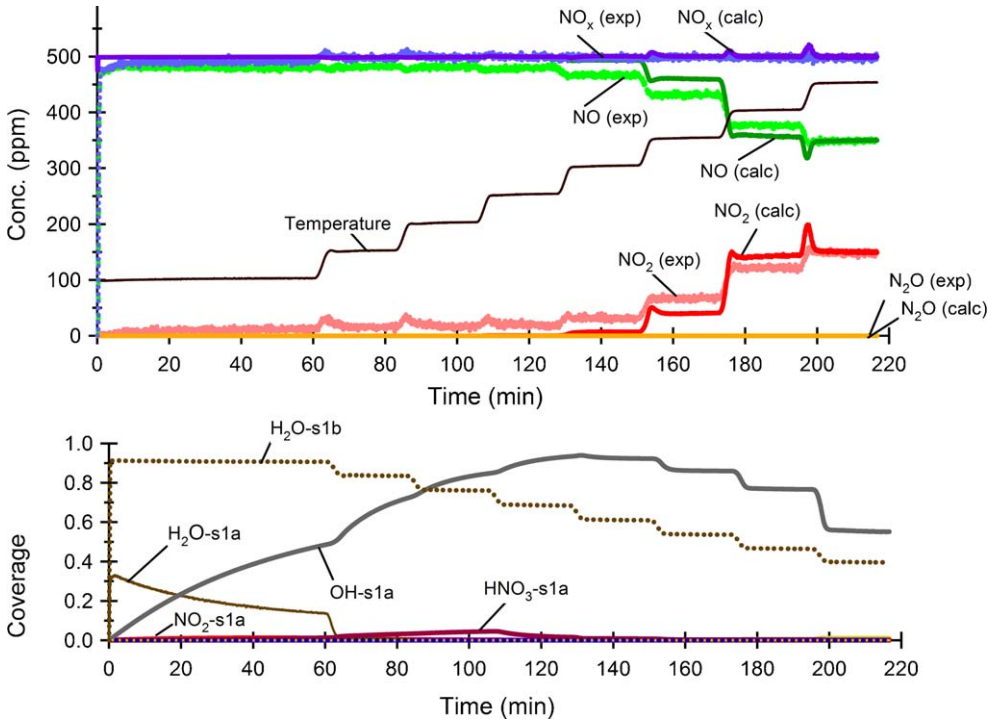

Fig. 7. Upper panel: Measured and calculated concentrations during NO oxidation experiment with 500 ppm NO, 8% O_2 and 5% H_2O and increasing the temperature stepwise. Dotted lines show the measured concentration and solid lines show the calculated concentration. Lower panel: Calculated mean coverage on S1a and S1b.

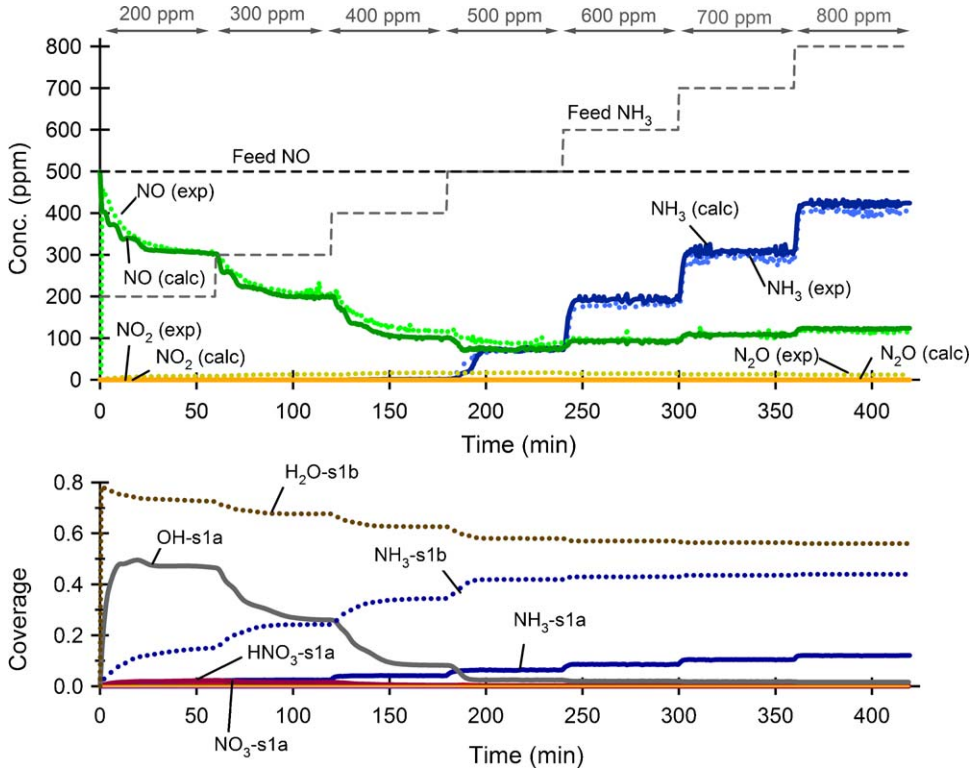

Fig. 8. Upper panel: Measured and calculated concentrations during NH_3 SCR experiment increasing the inlet NH_3 concentration in steps in humid feed at 175 °C, using Cu-ZSM-5-a. Feed condition: 200–800 ppm NH_3, 500 ppm NO, 8% O_2 and 5% H_2O. Dotted lines show the measured concentration and solid lines show the calculated concentration. Lower panel: Calculated mean coverage on S1a and S1b.

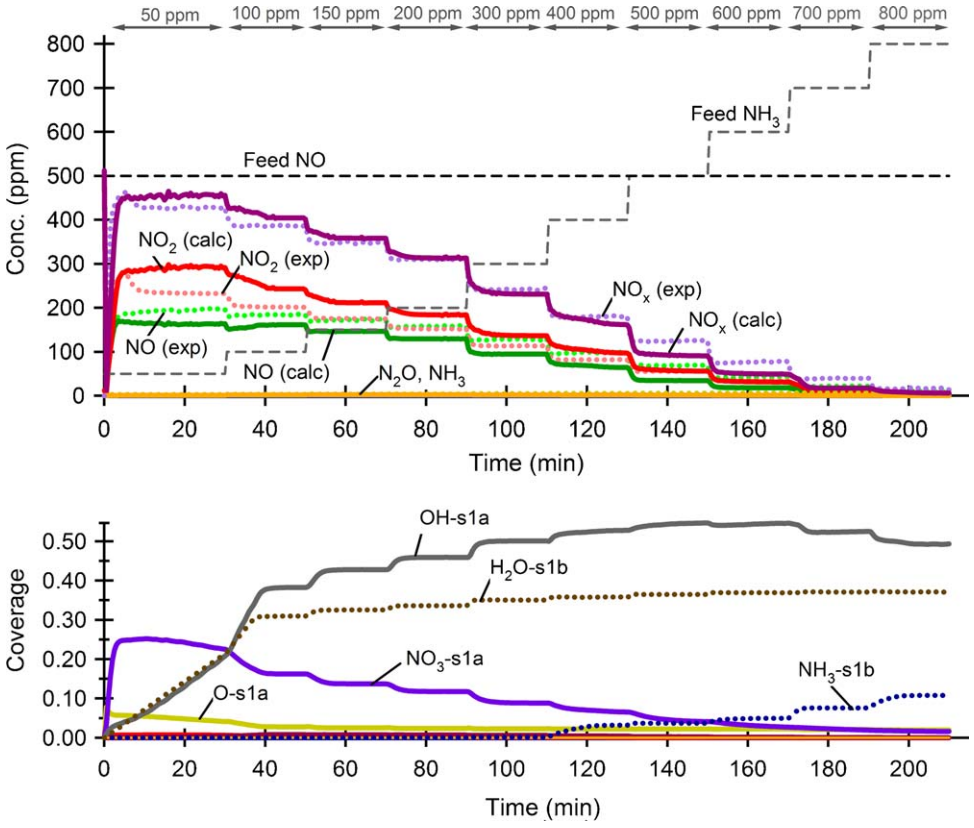

Fig. 9. Upper panel: Measured and calculated concentrations during NH_3 SCR experiment increasing the inlet NH_3 concentration in steps in dry feed at 350 °C, using Cu-ZSM-5-a. Feed condition: 50–800 ppm NH_3, 500 ppm NO and 8% O_2. Dotted lines show the measured concentration and solid lines show the calculated concentration. Lower panel: Calculated mean coverage on S1a and S1b.

some ammonia is observed on the surface, but the coverage is too low to cause inhibition on the reduction of NO_x. The model describes the enhanced NO_x reduction well and predicts the complete conversion of NH_3 observed.

An experiment was performed at 175 °C exposing the Cu-ZSM-5-b catalyst to 250 ppm NO, 250 ppm NO_2, 8% O_2, 5% H_2O and an NH_3 concentration increased stepwise from 200 ppm to 800 ppm. It is likely that ammonia inhibits the formation of surface NO_x, but if NO_2 is introduced directly via the feed, the activity is not expected to decrease since the oxidation of NO becomes less important. The result is shown in Fig. 10, where the reduction of NO_x increases with higher ammonia levels and reaches a complete conversion at stoichiometric concentration of NO_x and NH_3. The addition of higher feed concentrations of ammonia does not affect the conversion of NO_x. The surface coverage of each of the different NO_x species is stable and the coverage of NH_3 is low. Since the reduction rate is rapid, the consumption of ammonia is high and the surface coverage does not increase to levels where inhibition becomes important. Formation of about 50 ppm N_2O is detected and an ammonia slip is observed at high feed concentrations of NH_3, which is captured by the model. The model also predicts both the enhanced activity and the N_2O formation well.

Another experiment was carried out to study the effect of increasing ammonia concentrations in a mixture of NO and NO_2 at a higher temperature (350 °C) using Cu-ZSM-5-a. The experiment was made using a feed with 250 ppm NO, 250 ppm NO_2, 8% O_2 and with NH_3 concentrations increased stepwise from 50 ppm to 800 ppm. The oxidation of NO is rapid at this high temperature, which influences the ratio between NO and NO_2, and the experimental results presented in Fig. 11 are very similar to the experiment conducted using only NO (Fig. 9). An increased feed concentration of ammonia results in enhanced NO_x reduction activity without causing an ammonia slip, and the model predictions agree well with the experimental data. The surface coverage of NO_3 decreases with increased feed NH_3 concentration since more NO_x is consumed by the reaction and the coverage of H_2O increases as more water is formed.

The model was also validated using experiments with a constant (500 ppm) feed concentration of NH_3, but increasing concentration of NO. Experiments increasing the NO concentration from 50 ppm to 800 ppm were conducted at both 175 °C and 350 °C using Cu-ZSM-5-a. As expected, an increased consumption of ammonia is observed at 175 °C as more NO is fed to the reactor (Fig. 12). The concentration of NO out from the reactor increase with the feed concentration of NO since the conversion of NO is less than 100%. However, at 600 ppm NO, an enhanced NO reduction is observed because of the increased consumption of NH_3 which results in reduced ammonia coverage. The ammonia inhibition is active if equal or higher amounts of NH_3 compared to NO are used at this temperature (see Fig. 6), and the increased NO conversion at 600 ppm is likely caused by the reduced ammonia blocking effect. At 700 ppm and 800 ppm NO, all ammonia is consumed and any additional NO cannot be reduced. The model overestimates the NO conversion at low NO levels, but underestimates the reduction activity at high NO concentrations. However, the model did describe a higher outlet NO concentration and increased NH_3 consumption as more NO was fed to the reactor. In addition, a similar experiment was modeled at 350 °C and as shown in Fig. 13, the model was able to predict the experimental result more adequately at this high temperature. The model overestimates the NO conversion at the highest NO fractions slightly, but both the experimental and calculated result

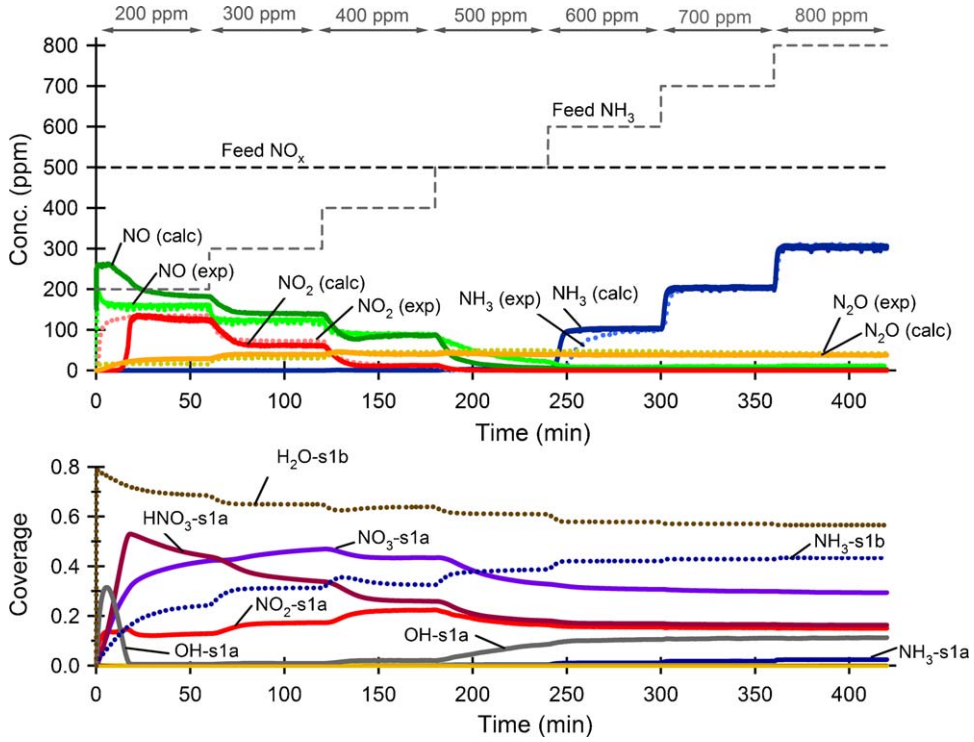

Fig. 10. Upper panel: Measured and calculated concentrations during NH_3 SCR experiment in wet feed with equal amounts of NO and NO_2, increasing the inlet NH_3 concentration in steps at 175 °C, using Cu-ZSM-5-b. Feed condition: 200–800 ppm NH_3, 250 ppm NO, 250 ppm NO_2, 8% O_2 and 5% H_2O. Dotted lines show the measured concentration and solid lines show the calculated concentration. Lower panel: Calculated mean coverage on S1a and S1b.

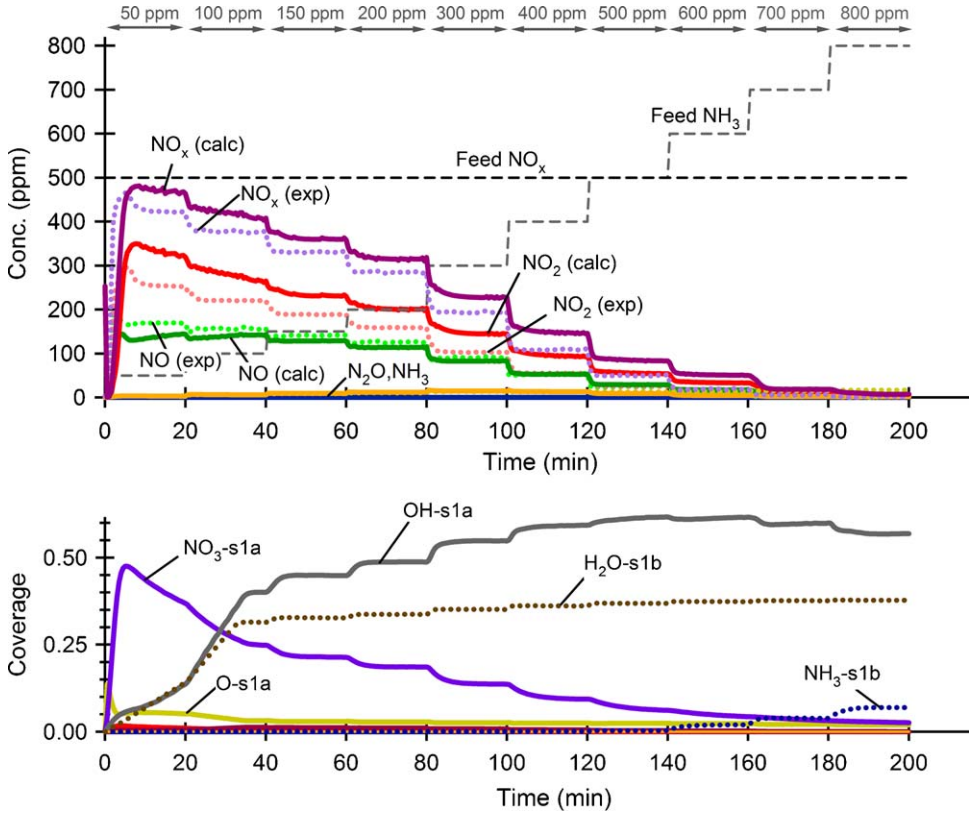

Fig. 11. Upper panel: Measured and calculated concentrations during NH_3 SCR experiment in dry feed with equal amounts of NO and NO_2, and increasing the inlet NH_3 concentration in steps at 350 °C using Cu-ZSM-5-a. Feed condition: 50–800 ppm NH_3, 250 ppm NO, 250 ppm NO_2 and 8% O_2. Dotted lines show the measured concentration and solid lines show the calculated concentration. Lower panel: Calculated mean coverage on S1a and S1b.

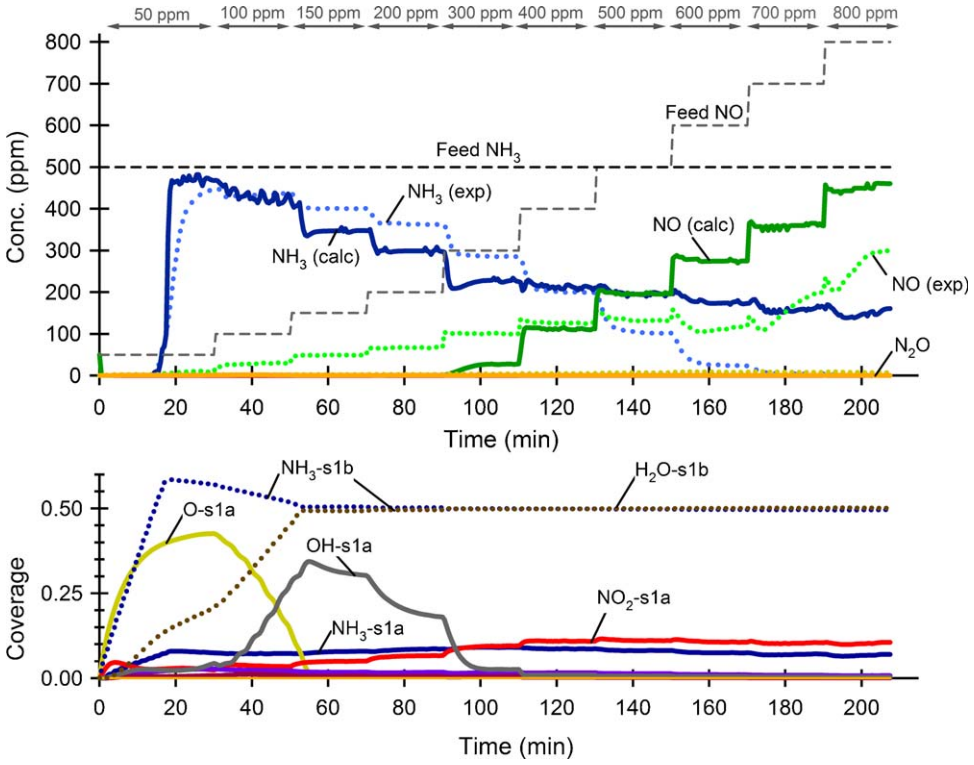

Fig. 12. Upper panel: Measured and calculated concentrations during NH_3 SCR experiment increasing the inlet NO concentration in steps in dry feed at 175 °C using Cu-ZSM-5-a. Feed condition: 50–800 ppm NO, 500 ppm NH_3 and 8% O_2. Dotted lines show the measured concentration and solid lines show the calculated concentration. Lower panel: Calculated mean coverage on S1a and S1b.

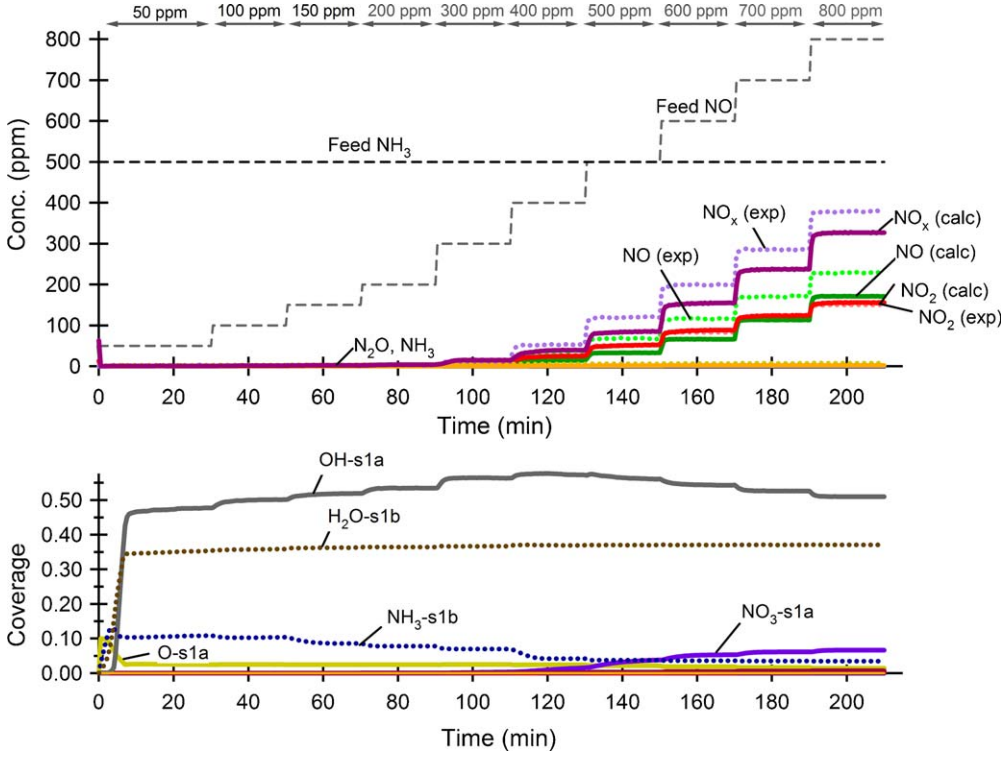

Fig. 13. Upper panel: Measured and calculated concentrations during NH_3 SCR experiment increasing the inlet NO concentration in steps in dry feed at 350 °C, using Cu-ZSM-5-a. Feed condition: 50–800 ppm NO, 500 ppm NH_3 and 8% O_2. Dotted lines show the measured concentration and solid lines show the calculated concentration. Lower panel: Calculated mean coverage on S1a and S1b.

indicates that no ammonia inhibition is observed, and the NO reduction activity is high.

5. Conclusions

The SCR activity was modeled using detailed kinetic models previously developed for two subsystems. The first subsystem describes the catalyst surface, ammonia storage and oxidation, both with and without the presence of water. The second subsystem describes the NO_x adsorption and NO oxidation. The two subsystems were combined and additional reactions were added to account for the SCR activity. The model includes four steps for the selective catalytic reduction of NO_x. The initial reaction in the SCR was assumed to occur between adsorbed NO_2 and NH_3 followed by reactions forming either HNO_2 or HNO_3, which subsequently reacts with NH_3 to produce N_2 or N_2O and H_2O.

The kinetic parameters for the NO oxidation subsystem were kept constant as determined from our earlier study. However, there was a large correlation between the SCR reaction steps and NH_3 storage and oxidation. These steps were therefore fitted simultaneously using 13 experiments (NH_3 and H_2O TPD experiments, NH_3 oxidation experiments with and without water, NO oxidation with water and six SCR experiments). The selective catalytic reduction of NO was modeled in both dry and wet feed at temperatures from 100 °C to 500 °C. The effect of varying the NO to NO_2 ratio at 175 °C was also included in both dry and wet feed as well as an ammonia inhibition experiment at the same temperature. The NO to NO_2 ratio was investigated at a higher temperature and finally NO oxidation in the presence of water. The model was able to describe the ammonia adsorption and desorption and the SCR activity over the wide range of temperatures considered. The effect of introducing NO_2 as a fraction of total NO_x was also modeled successfully. The ammonia inhibition was modeled as a competition between ammonia storage and formation of other surface species that are important for the reduction of NO_x, and the result correlated well with the experiment at the investigated temperature. Six separate experiments were conducted to validate the model. The model was validated at both 175 °C and 350 °C under various feedstream conditions and was able to predict most of the experimental results well.

In summary, this model was developed to account for the SCR of NO and NO_2 using a detailed mechanism instead of the more commonly used global expression for the "standard SCR", "fast SCR" and the SCR of NO_2. Various combinations of the steps in this detailed mechanism will add up to various summary reactions earlier reported in the literature. This detailed model may help to increase the understanding of the elementary steps in the SCR of NO_x with ammonia. It is able to describe the ammonia storage and oxidation, the role of NO and NO_2, the ammonia inhibition and the effect of introducing water into the feed.

Acknowledgements

The work is performed at Competence Centre for Catalysis (KCK), Chalmers and at General Motors Research and Development Center. The authors would like to acknowledge helpful discussions with Se Oh, Ed Bissett, Jong-Hwan Lee, Byong Cho and Steven J. Schmieg of the General Motors Research and Development Center and Ashok Gopinath at GM ISL. We would also like to thank GM R&D Center for the financial support. One author (Louise Olsson) would also like to acknowledge the Swedish Research Council (Contract: 621-2003-4149 and 621-2006-3706) for additional support.

References

[1] N.-Y. Topsoe, H. Topsoe, J.A. Dumesic, J. Catal. 151 (1995) 226–240.
[2] J.A. Dumesic, N.-Y. Topsoe, H. Topsoe, Y. Chen, T. Slabiak, J. Catal. 163 (1996) 409–417.
[3] I.E. Wachs, G. Deo, B.M. Weckhuysen, A. Andreini, M.A. Vuurman, M.d. Boer, M.D. Amiridis, J. Catal. 161 (1996) 211–221.
[4] B. Roduit, A. Wokaun, A. Baiker, Ind. Eng. Chem. Res. 37 (1998) 4577–4590.
[5] E. Tronconi, I. Nova, C. Ciardelli, D. Chatterjee, B. Bandl-Konrad, T. Burkhardt, Catal. Today 105 (2005) 529–536.
[6] C. Ciardelli, I. Nova, E. Tronconi, D. Chatterjee, B. Bandl-Konrad, M. Weibel, B. Krutzsch, Appl. Catal., B 70 (2007) 80–90.
[7] E. Tronconi, I. Nova, C. Ciardelli, D. Chatterjee, M. Weibel, J. Catal. 245 (2007) 1–10.
[8] T. Komatsu, M. Nunokawa, I.S. Moon, T. Takahara, S. Namba, T. Yashima, J. Catal. 148 (1994) 427–437.
[9] K. Rahkamaa-Tolonen, T. Maunula, M. Lomma, M. Huuhtanen, R.L. Keiski, Catal. Today 100 (2005) 217–222.
[10] J.H. Baik, S.D. Yim, I.S. Nam, Y.S. Mok, J.H. Lee, B.K. Cho, S.H. Oh, Top. Catal. 30–31 (2004) 37–41.
[11] S.J. Schmieg, J.-H. Lee, SAE Technical Paper, 2005-01-3881, 2005.
[12] H. Sjövall, L. Olsson, E. Fridell, R.J. Blint, Appl. Catal., B 64 (2006) 180–188.
[13] O. Kröcher, M. Devadas, M. Elsener, A. Wokaun, N. Söger, M. Pfeifer, Y. Demel, L. Mussmann, Appl. Catal., B 66 (2006) 208–216.
[14] H. Sjövall, E. Fridell, R.J. Blint, L. Olsson, Top. Catal. 42–43 (2007) 113–117.
[15] M. Devadas, O. Kröcher, M. Elsener, A. Wokaun, N. Söger, M. Pfeifer, Y. Demel, L. Mussmann, Appl. Catal., B 67 (2006) 187–196.
[16] J.-H. Park, H.J. Park, J.H. Baik, I.-S. Nam, C.-H. Shin, J.-H. Lee, B.K. Cho, S.H. Oh, J. Catal. 240 (2006) 47–57.
[17] M. Schwidder, M.S. Kumar, K. Klementiev, M.M. Pohl, A. Bruckner, W. Grunert, J. Catal. 231 (2005) 314–330.
[18] G. Centi, S. Perathoner, Appl. Catal., A 132 (1995) 179–259.
[19] M. Shelef, Chem. Rev. 95 (1995) 209–225.
[20] V.I. Parvulescu, P. Grange, B. Delmon, Catal. Today 46 (1998) 233–316.
[21] A. Fritz, V. Pitchon, Appl. Catal., B 13 (1997) 1–25.
[22] M. Koebel, M. Elsener, M. Kleemann, Catal. Today 59 (2000) 335–345.
[23] M. Koebel, G. Madia, M. Elsener, Catal. Today 73 (2002) 239–247.
[24] M. Koebel, G. Madia, F. Raimondi, A. Wokaun, J. Catal. 209 (2002) 159–165.
[25] S.A. Stevenson, J.C. Vartuli, J. Catal. 208 (2002) 100–105.
[26] M. Koebel, M. Elsener, G. Madia, Ind. Eng. Chem. Res. 40 (2001) 52–59.
[27] G. Busca, L. Lietti, G. Ramis, F. Berti, Appl. Catal., B 18 (1998) 1–36.
[28] J. Eng, C.H. Bartholomew, J. Catal. 171 (1997) 27–44.
[29] T. Komatsu, T. Ogawa, T. Yashima, J. Phys. Chem. 99 (1995) 13053–13055.
[30] Y.H. Yeom, J. Henao, M.J. Li, W.M.H. Sachtler, E. Weitz, J. Catal. 231 (2005) 181–193.
[31] E.-Y. Choi, I.-S. Nam, Y.G. Kim, J. Catal. 161 (1996) 597–604.
[32] Q. Sun, Z.-X. Gao, B. Wen, W.M.H. Sachtler, Catal. Lett. 78 (2002) 1–5.
[33] J.R. Kiovsky, P.B. Koradia, C.T. Lim, Ind. Eng. Chem. Prod. Res. Dev. 19 (1980) 218–225.
[34] S.A. Stevenson, J.C. Vartuli, C.F. Brooks, J. Catal. 190 (2000) 228–239.
[35] M. Wallin, C.J. Karlsson, M. Skoglundh, A. Palmqvist, J. Catal. 218 (2003) 354–364.
[36] M. Richter, R. Eckelt, B. Parlitz, R. Fricke, Appl. Catal., B 15 (1998) 129–146.
[37] I. Nova, C. Ciardelli, E. Tronconi, D. Chatterjee, B. Bandl-Konrad, Catal. Today 114 (2006) 3–12.
[38] A. Grossale, I. Nova, E. Tronconi, D. Chatterjee, M. Weibel, J. Catal. 256 (2008) 312–322.
[39] G. Delahay, S. Kieger, N. Tanchoux, P. Trens, B. Coq, Appl. Catal., B 52 (2004) 251–257.
[40] J.H. Baik, S.D. Yim, I.S. Nam, Y.S. Mok, J.H. Lee, B.K. Cho, S.H. Oh, Ind. Eng. Chem. Res. 45 (2006) 5258–5267.
[41] R. Willi, M. Maciejewski, U. Gobel, R.A. Koppel, A. Baiker, J. Catal. 166 (1997) 356–367.
[42] C. Ciardelli, I. Nova, E. Tronconi, B. Konrad, D. Chatterjee, K. Ecke, M. Weibel, Chem. Eng. Sci. 59 (2004) 5301–5309.
[43] D. Chatterjee, T. Burkhardt, B. Bandl-Konrad, T. Braun, E. Tronconi, I. Nova, C. Ciardelli, SAE Technical Paper, 2005-01-0965, 2005.
[44] J.C. Wurzenberger, R. Wanker, SAE Technical Paper, 2005-01-0948, 2005.
[45] S. Malmberg, M. Votsmeier, J. Gieshoff, N. Söger, L. Mußmann, A. Schuler, A. Drochner, Top. Catal. 42–43 (2007) 33–36.
[46] L. Olsson, H. Sjövall, R.J. Blint, Appl. Catal., B 81 (2008) 203–217.
[47] H. Sjövall, L. Olsson, R.J. Blint, J. Phys. Chem. C 113 (2009) 1393–1405.
[48] L. Olsson, H. Sjövall, R.J. Blint, Appl. Catal., B 87 (2009) 200–210.
[49] H.S. Fogler, Elements of Chemical Reaction Engineering, 3rd Ed., Prentice Hall PTR, Upper Saddle River, New Jersey, 1999.
[50] B. Westerberg, C. Künkel, C.U.I. Odenbrand, Chem. Eng. J. 92 (2003) 27–39.
[51] B.E. Poling, J.M. Prausnitz, J.P. O'Connell, The Properties of Gases and Liquids, 5 Ed., McGraw-Hill, New York, 2000.
[52] E. Tronconi, P. Forzatti, AIChE J. 38 (1992) 201–210.
[53] B. Coq, G. Delahay, R. Durand, D. Berthomieu, E. Ayala-Villagomez, J. Phys. Chem. B 108 (2004) 11062–11068.
[54] S. Brandenberger, O. Kröcher, A. Tissler, R. Althoff, Catal. Rev. 50 (2008) 492–531.
[55] S. Kieger, G. Delahay, B. Coq, B. Neveu, J. Catal. 183 (1999) 267–280.
[56] S.W. Ham, H. Choi, I.-S. Nam, Y. Kim, Catal. Lett. 42 (1996) 35–40.
[57] W.B. Williamson, D.R. Flentge, J.H. Lunsford, J. Catal. 37 (1975) 258–266.
[58] W.B. Williamson, J.H. Lunsford, J. Phys. Chem. 80 (1976) 2664–2671.
[59] A. Delabie, K. Pierloot, M.H. Groothaert, B.M. Weckhuysen, R.A. Schoonheydt, Microporous Mesoporous Mater. 37 (2000) 209–222.
[60] A. Grossale, I. Nova, E. Tronconi, Catal. Today 136 (2008) 18–27.

[61] I. Nova, C. Ciardelli, E. Tronconi, D. Chatterjee, M. Weibel, Top. Catal. 42–43 (2007) 43–46.
[62] C. Ciardelli, I. Nova, E. Tronconi, D. Chatterjee, T. Burkhardt, M. Weibel, Chem. Eng. Sci. 62 (2007) 5001–5006.
[63] N.Y. Topsoe, K. Pedersen, E.G. Derouane, J. Catal. 70 (1981) 41–52.
[64] B. Hunger, J. Hoffmann, Thermochim. Acta 106 (1986) 133–140.
[65] G.I. Kapustin, T.R. Brueva, A.L. Klyachko, S. Beran, B. Wichterlova, Appl. Catal. 42 (1998) 239–246.